Computer simulation of temperature-dependent growth of fractal and compact domains in diluted Ising models

Sørensen, Erik Schwartz; Fogedby, Hans C.; Mouritsen, Ole G.

Published in:
Physical Review A (Atomic, Molecular and Optical Physics)

Link to article, DOI:
10.1103/PhysRevA.39.2194

Publication date:
1989

Document Version
Publisher's PDF, also known as Version of record

Computer simulation of temperature-dependent growth of fractal and compact domains in diluted Ising models

Erik Schwartz Sørensen and Hans C. Fogedby
Institute of Physics, Aarhus University, DK-8000 Aarhus C, Denmark

Ole G. Mouritsen
Department of Structural Properties of Materials, The Technical University of Denmark, Building 307, DK-2800 Lyngby, Denmark

(Received 12 September 1988)

A version of the two-dimensional site-diluted spin-$\frac{1}{2}$ Ising model is proposed as a microscopic interaction model which governs solidification and growth processes controlled by vacancy diffusion. The Ising Hamiltonian describes a solid-fluid phase transition and it permits a thermodynamic temperature to be defined. The dynamics of the model are taken to involve (i) solid-fluid conversion and (ii) diffusion of vacancies in the fluid phase. By means of Monte Carlo computer-simulation techniques the solidification and growth processes following rapid thermal quenches below the transition temperature are studied as functions of temperature, time, and concentration. At zero temperature and high dilution, the growing solid is found to have a fractal morphology and the effective fractal exponent D varies with concentration and ratio of time scales of the two dynamical processes. The mechanism responsible for forming the fractal solid is shown to be a buildup of a locally high vacancy concentration in the active growth zone. The growth-probability measure of the fractals is analyzed in terms of multifractality by calculating the $f(\alpha)$ spectrum. It is shown that the basic ideas of relating probability measures of static fractal objects to the growth-probability distribution during formation of the fractal apply to the present model. The $f(\alpha)$ spectrum is found to be in the universality class of diffusion-limited aggregation. At finite temperatures, the fractal solid domains become metastable and a crossover to compact equilibrium solidification is observed as a function of both temperature and time. At low temperatures in the metastable fractal growth regime, the time dependence of the particle content of the domains is found to obey the scaling law, $N(t) \sim t^{D/(2d-D-1)}$. At higher temperatures where the growth is stable and leads to compact domains, the time dependence of $N(t)$ can be described by a simple hyperbolic function. The various results of the theoretical model study are related to fractal and compact growth patterns observed in experimental studies of impure lipid monolayer films at air-water interfaces.

I. INTRODUCTION

Recent studies of physical systems exhibiting fractal growth patterns have made it increasingly clear that fractal morphology is often a consequence of a transient phenomenon in either space or time and that true fractal geometry only arises under very special circumstances. The celebrated case of standard diffusion-limited aggregation[1] (DLA) is probably such a special case although—despite the simplicity of the DLA process—neither the exact fractal dimension of DLA nor the large-scale properties of DLA aggregates are known. Some progress has, however, been attained recently via exact solutions to equipotential lines of deterministically generated Julia sets of mappings in the complex plane.[2,3] These studies indicate that there exists an analytical representation of DLA in terms of certain Julia sets.

Notwithstanding the fundamental problems regarding the circumstances under which exact fractal behavior arises in physical systems, there is ample theoretical and experimental[4] evidence that growth patterns are effectively fractal over finite length scales and finite time spans. These facts make studies of crossover from fractal behavior to nonfractal behavior of particular importance. Experimentally, such crossover has been studied in the spatial regime[5] and to some extent also in the time regime, for example, for colloids where restructuring and compactification of an initially fractal structure has been observed.[6,7]

Theoretically, crossover from fractal morphology to compact structures or to a fractal morphology with different characteristics has been studied analytically and numerically as a function of spatial parameters, e.g., crossover from fractal to dendritic growth as a result of competition between diffusion and field,[8] crossover to dendritic pattern formation in the presence of anisotropy,[9–12] crossover to dense branching morphology for weak anisotropy and finite surface tension,[10] and crossover between a variety of morphologies by varying model parameters in DLA-like growth models.[11–21]

The fractal morphology in many of the theoretical models is a consequence of a nonequilibrium condition which is introduced either as a persistent intrinsic irreversibility or an effective zero-temperature condition.

By lifting this nonequilibrium condition, the system will eventually change morphology and compactify as it approaches thermodynamic equilibrium. A study of this crossover in temperature and time is of significance since it is relevant for the interpretation of experimental investigations of the kinetics of pattern formation.

However, a study of temporal and thermal crossovers is difficult since it requires a Hamiltonian formalism to permit definition of a thermodynamic temperature. We have recently[22] given a brief account of some results from the first numerical-simulation study of the crossover from nonequilibrium fractal growth to equilibrium compact growth by using a microscopic interaction model capable of accounting for solidification on a lattice. In this paper we shall give a detailed description of the results obtained from this model, which not only governs a spontaneous thermally driven ordering process, but moreover, controls the full scenario from nucleation, fractal growth, and coarsening of the ordered domains, to equilibrium compactification. The model study of Shih *et al.*[23] on cluster-cluster aggregation with finite binding energies is related to our study in that it provides a mechanism for thermal equilibration via temperature-dependent sticking probabilities. However, that study does not involve a Hamiltonian which drives the cooperative phenomenon. Similarly, the reversible DLA models which allow for disaggregation processes[24,25] are also related to the present work in that they lead to equilibrium structures. For these models, however, this equilibrium is a constrained kinetic equilibrium and is not governed by thermodynamics. The fractal properties of growing droplets nucleated near the classical spinodal have recently been described by field theory and computer simulation.[26]

Our model study has been motivated and stimulated by the recent experimental activity in the field of nonequilibrium solidification and growth processes in condensed phases of lipid monolayers spread on air-water interfaces. Rapidly compressed lipid monolayers doped with a fluorescent dye impurity miscible only in the fluid phase are found to support solid domain patterns as well as fractal or dendritic structures,[27,28] depending on the experimental circumstances. In these monolayers, it turns out to be the diffusion of the dye impurity, rather than diffusion of latent heat, which is responsible for the tenuous solid domains.[27–30]

The Hamiltonian on which our model study is based is presented in Sec. II and the computational techniques employed to derive the properties of the growth model are outlined in Sec. III. Due to the very different time scales of the various processes involved continuum-time Monte Carlo methods have to be invoked as well as vectorized algorithms. A major part of the paper, Sec. IV, is devoted to zero-temperature growth phenomena and how the morphology might depend on the various model parameters, i.e., vacancy concentration and relative time scales of the dynamical processes. The multifractal properties and the $f(\alpha)$ spectrum of the zero-temperature morphologies are discussed in Sec. V. The approach to equilibrium is studied in Sec. VI, where crossover in temperature as well as time is considered. The paper is concluded with a discussion in Sec. VII.

II. MODEL

A. Hamiltonian

As a simple statistical mechanical model of a solid-fluid phase transition on a lattice we have adopted the two-state model of Doniach.[31] This model is formulated in terms of spin-$\frac{1}{2}$ Ising variables, $\sigma_i = \pm 1$, where $\sigma_i = +1$ refers to the fluid state and $\sigma_i = -1$ refers to the solid state. The two states are assigned different internal degeneracies, $D_{+1} \gg D_{-1}$, and internal energies, $E_{+1} > E_{-1} = 0$. The Hamiltonian is given by

$$H = -\sum_i h(T)(1+\sigma_i) - J \sum_{\langle i,j \rangle} (1-\sigma_i)(1-\sigma_j) , \tag{1}$$

with $J > 0$ and where the summation is taken over nearest-neighbor pairs of a square lattice. The temperature-dependent field

$$h(T) = -\tfrac{1}{2}(E_{+1} - k_B T \ln D_{+1}) \tag{2}$$

provides the driving force for a phase transition from a low-temperature phase characterized by particles predominantly in the $\sigma_i = -1$ state (the solid phase) to a high-temperature phase characterized by particles predominantly in the $\sigma_i = +1$ state (the fluid phase). This transition is of first order provided that $h(T^*) = 0$ for $T^* < T_c$, where T_c is the critical temperature of the two-dimensional zero-field Ising model,[31] $k_B T_c / J = 0.567\,296\,3z$ (z is the coordination number of the lattice). Since the first-order transition is driven by the difference in internal entropy,

$$\Delta S = k_B \ln(D_{+1}/D_{-1}) ,$$

between the two single-particle states, we can at low temperatures directly relate the particle state to the thermodynamic phase.

The site-diluted version of the model is now written

$$H = -\sum_i h(T)(1+\sigma_i)\eta_i - J \sum_{\langle i,j \rangle} (1-\sigma_i)(1-\sigma_j)\eta_i \eta_j , \tag{3}$$

where we have introduced the occupation variables $\eta_i = 0, 1$. The particle concentration is then $\langle \eta_i \rangle$. The dilution will lower the transition temperatures of the system and eventually, below the percolation limit ($\langle \eta_i \rangle \simeq 0.59$ for the square lattice) remove the transition in the homogeneous system. Even above the percolation limit some cooperativity remains and the system will at low temperatures condense into solid domains of finite size.

B. Model dynamics and transition classes

The Ising Hamiltonian of Eq. (3) has no dynamics of its own and we therefore associate it with dynamical processes consisting of a combination of two types of transitions: (a) Glauber-type single-site solid-fluid conversion, $\sigma_i = 1 \leftrightarrow \sigma_i = -1$ and (b) Kawasaki-type nearest-neighbor exchange of fluid particles and vacancies (diffusion). We

do not allow particles in the solid state to diffuse. This dynamics, which schematically is illustrated in Fig. 1, leads naturally to 15 different transition classes as listed in Table I. Classes 1–10 correspond to Glauber-type dynamics and classes 11–15 to Kawasaki-type diffusional dynamics.

The transition probabilities for the various transitions are determined by the usual Metropolis Monte Carlo criterion[32] for finite temperatures,

$$\Pi_m(T>0)=\tau^{-1}e^{-\Delta E_m/k_BT}$$

for transition energy $\Delta E_m>0$, and

$$\Pi_m(T>0)=1$$

for $\Delta E_m\leq 0$. The quantity τ sets the characteristic time scale of the process in question, denoted specifically τ_S and τ_D for the solidification and diffusion processes, respectively. In the case of diffusional motion, which per definition is restricted to particles in the fluid state, $\Delta E=0$ and the transition probability is taken to be proportional to the number of vacant sites to which the fluid particle can move. At zero temperature only transitions involving $\Delta E\leq 0$ are allowed. Hence in this limit once clusters with more than one solid particle have formed, they cannot fluidize again. This is the limit of irreversible solid-solid aggregation[29] which is solely governed by the competition between nonactivated processes on the two time scales τ_S and τ_D. A special remark should be made regarding class 10 of Table I. Class 10 involves formation of single-site clusters in the solid state. At zero temperature this is taken to be forbidden and hence the growth process can only be initiated by introducing a seed of solid. Such a procedure has obvious computational advantages. At nonzero temperature, processes in class 10 are activated and they involve a certain nucleation barrier of energy ΔE_{10}.

In the zero-temperature limit, the present model is related to the multiparticle diffusion-limited aggregation models[13,14] in that many particles diffuse at the same time. However, there is an important difference in that in our model, only one particle at a time can stick to the aggregate and a fluid particle which finds itself at a nearest-neighbor position to solid particles in the current aggregate does only stick if it at the same time undergoes a fluid-solid transition. Hence, in the zero-temperature limit, the ratio of time scales τ_S/τ_D for solidification and

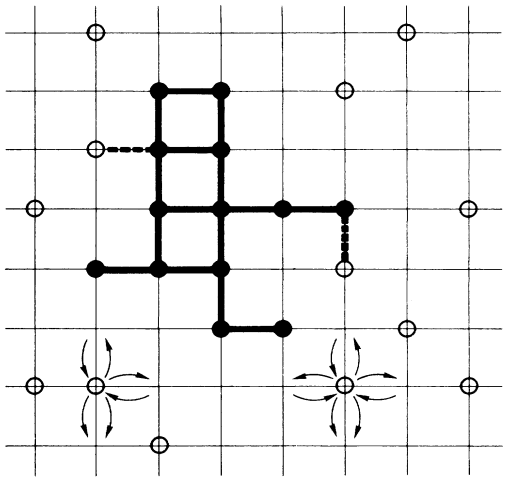

FIG. 1. Schematic illustration of the dynamical processes of the model. Particles on the square lattice are denoted by solid circles for particles in the solid state ($\sigma_i=-1$) and by open circles for particles in the fluid state ($\sigma_i=+1$). Bonds between solidified (aggregated) particles are indicated by heavy solid lines and possible candidates for formation of new bonds are connected by dashed lines. Arrows indicate for some fluid particles possible directions of diffusive motion.

TABLE I. Transition classes 1–15 for transitions involving single-site solid-fluid conversion, 1–10, and vacancy diffusion, 11–15. n_- denotes the number of neighboring particles in the solid state and $n_{\rm vac}$ denotes the number of vacant neighboring sites. ΔE_m is the transition energy and $\Pi_m(T>0)$ and $\Pi_m(T=0)$ are the transition probabilities at finite and zero temperatures, respectively.

Class m	Transition	n_-	$n_{\rm vac}$	ΔE_m	$\Pi_m(T>0)$	$\Pi_m(T=0)$
1	$-\rightarrow+$	4		$32J-2h(T)$	$\tau_S^{-1}e^{-\Delta E_m/k_BT}$	0
2	$-\rightarrow+$	3		$24J-2h(T)$	$\tau_S^{-1}e^{-\Delta E_m/k_BT}$	0
3	$-\rightarrow+$	2		$16J-2h(T)$	$\tau_S^{-1}e^{-\Delta E_m/k_BT}$	0
4	$-\rightarrow+$	1		$8J-2h(T)$	$\tau_S^{-1}e^{-\Delta E_m/k_BT}$	0
5	$-\rightarrow+$	0		$-2h(T)$	$\tau_S^{-1}e^{-\Delta E_m/k_BT}$	0
6	$+\rightarrow-$	4		$-32J+2h(T)$	$\tau_S^{-1}e^{-\Delta E_m/k_BT}$	τ_S^{-1}
7	$+\rightarrow-$	3		$-24J+2h(T)$	$\tau_S^{-1}e^{-\Delta E_m/k_BT}$	τ_S^{-1}
8	$+\rightarrow-$	2		$-16J+2h(T)$	$\tau_S^{-1}e^{-\Delta E_m/k_BT}$	τ_S^{-1}
9	$+\rightarrow-$	1		$-8J+2h(T)$	$\tau_S^{-1}e^{-\Delta E_m/k_BT}$	τ_S^{-1}
10	$+\rightarrow-$	0		$2h(T)$	$\tau_S^{-1}e^{-\Delta E_m/k_BT}$	0
11	$+\leftrightarrow$vac		0		0	0
12	$+\leftrightarrow$vac		1		$\tau_D^{-1}/4$	$\tau_D^{-1}/4$
13	$+\leftrightarrow$vac		2		$\tau_D^{-1}/2$	$\tau_D^{-1}/2$
14	$+\leftrightarrow$vac		3		$3\tau_D^{-1}/4$	$3\tau_D^{-1}/4$
15	$+\leftrightarrow$vac		4		τ_D^{-1}	τ_D^{-1}

diffusion processes becomes a key parameter. At finite temperatures, the present model bears some resemblance to the cluster-cluster aggregation models with finite binding energy and time-scale parameters governing unbinding and diffusion.[23] However, the model of Shih *et al.*[23] does not involve a Hamiltonian and hence the "temperature parameter" in their sticking probabilities is not a thermodynamic temperature.

The parameters of the Hamiltonian, Eqs. (2) and (3), are chosen to be $E_{+1}=2.42J$ and $D_{+1}=10^9$. For these parameter values, the growth phenomena we want to study occur at length and time scales which are agreeable with our computer capacity. Other choices of these parameters lead to results similar to those reported below.

III. COMPUTATIONAL TECHNIQUES

The spatial and temporal properties of the model defined by Eqs. (2) and (3) and Table I are simulated by stochastic Metropolis Monte Carlo sampling.[32] For $T=0$, the sampling reduces to that characteristic of irreversible aggregation models. The simulations are carried out on finite lattices subject to periodic boundary conditions. A variety of lattice sizes have been studied ranging from 100×100 to 1024×1024 sites. The major part of the results reported below is derived from a 256×256 square lattice. The aggregates grown involve particles in numbers ranging typically from 5×10^3 to 2×10^5. Depending on the temperature and the time-scale ratio τ_S/τ_D, the aggregates are often grown beyond a point where all particles have solidified.

From the finite-temperature transition probabilities of the nondiffusive processes listed in Table I it is anticipated that at a given temperature the transition frequency for fluidizing (detaching) double- and triple-bound solid particles will be orders of magnitude lower than that of single-bound particles. Hence we have supplemented the conventional Metropolis Monte Carlo sampling characterized by a discrete time parameter (measured in units of Monte Carlo steps per site, MCS/S) with a version of the continuum-time method of Bortz *et al.*[33] According to this method, each trial transition is successful and the time parameter is subsequently updated by a continuous amount which is determined by calculating the expected lifetime of the preceding configuration. The method requires a classification of the particles according to the local field they experience, i.e., precisely the classification of Table I. The probability of performing a transition belonging to a certain class, m, is then taken to be $p_m=N_m\Pi_m$, where N_m is the number of particles of the given configuration which belong to class m. The total probability is therefore

$$Q=\sum_{m=1}^{15} p_m \ . \tag{4}$$

The continuum-time method is now implemented as follows. A random number between 0 and Q is drawn in order to select a class for updating. Another random number is generated to choose a particle in that class at random. The lifetime of the preceding state can then be computed as

$$\Delta t=-\frac{\tau}{Q}\ln\xi \ , \tag{5}$$

where ξ is a random number between 0 and 1 and $\tau=1$ MCS/S. After the transition has been performed, the time is incremented by Δt. The logarithmic function in Eq. (5) ensures that the lifetime is exponentially distributed with parameter Q/τ. We have tested our implementation of the continuum-time method against conventional updating and the results of the two methods are identical within the confidence limits. In the late-time regime, which is dominated by slow rearrangement processes, it is absolutely necessary to use powerful techniques such as the continuum-time method in order for the simulation to sample the phenomena of interest.

It should be mentioned that with the present choice of time parameter, which contains contributions from temperature-dependent Glauber-type transitions as well as temperature-independent Kawasaki-type transitions, we basically work with a temperature-dependent time-scale ratio of the two types of processes when $T>0$. It is possible to map this onto a temperature-independent time parameter if one keeps track of the full time series of transitions. We have not done this since we are in this work only concerned with the scaling properties of the time-dependent quantities. The time parameter is initiated at the occurrence of the first nucleation event.

For the purpose of determining the multifractal spectrum of the aggregates at zero temperature we have implemented a vectorized updating algorithm for the model. This was necessary in order to generate large enough aggregates and to obtain sufficient statistics for their probability measure (see Sec. V). The main problem with a vectorized algorithm is to account for the diffusive motion in a parallel way, i.e., several particles have to be moved simultaneously without getting multiple occupancy at any site. We get around this problem by dividing the lattice into a large number of equivalent interpenetrating square sublattices, each of which contains only noninteracting particles for any of the possible transitions of Table I. All particles at that sublattice are then updated simultaneously. This may be considered a random-serial updating mechanism where the ordinary algorithm is a random-random mechanism (choose a random sublattice and then move a single randomly chosen particle at that lattice). Hence, in the vectorized algorithm, the same particle cannot be chosen twice in a row for updating, in contrast to the ordinary algorithm. By choosing a sufficiently large number of sublattices, no effect of the underlying updating mechanism could be discerned.

IV. ZERO-TEMPERATURE FRACTAL GROWTH

At zero temperature the growth process is initiated by introducing a single small seed of particles in the solid state. Aggregates are then grown for a variety of time-scale ratios τ_S/τ_D and particle concentrations $\langle\eta_i\rangle$. Ensemble-average properties of the aggregates are obtained by averaging the results derived from different sequences of the random numbers used to simulate the stochastic nature of the solidification and diffusional pro-

cesses. In Fig. 2 are shown typical solid aggregates grown to a linear size of about 150 lattice units at particle concentration $\langle \eta_i \rangle = 0.3$ over five decades of the time-scale ratio τ_S/τ_D. Except for very fast diffusion the morphology of the aggregates appears very tenuous and characterized by tipslitting and a finger thickness which increases with τ_S/τ_D. The tipsplitting becomes less pronounced for faster diffusion. The patterns grown at $\tau_S/\tau_D \sim 1$ have an appearance similar to the fractal patterns of the standard DLA.[1]

The morphology of the solid aggregates is analyzed in terms of a fractal dimension D defined as

$$N(R) \sim R^D , \tag{6}$$

where $N(R)$ is the particle content in a region of the aggregate of linear extension R. Figure 3 presents a log-log plot of Eq. (6) for aggregates of the type in Fig. 2. The data are averaged over a large number of different aggregates. It is clearly seen that the aggregates are scale invariant and effectively described by a fractal exponent D over a wide range of distances. As expected, there are low-R and high-R cutoffs and associated crossover regions. For selected values of τ_S/τ_D we have grown much larger aggregates ($\sim 2\times 10^5$ particles) than those underlying the data of Fig. 3. The results for the large aggregates support the conclusions drawn from Fig. 3 and show that the fractal regime extends to long-length scales. The fractal exponent values obtained from the linear plots in Fig. 3 are plotted as a function of τ_S/τ_D in Fig. 4.

The variation of D with the time-scale ratio in Fig. 4 has a number of very striking features. Firstly, there is a distinct minimum around $\tau_S/\tau_D \sim 1$ where the value of D is around 1.7, which is close to the fractal dimension of two-dimensional DLA.[1] Secondly, for fast diffusion D approaches the Euclidean dimension, $d=2$, corresponding to compact aggregates. Thirdly, for slow diffusion, D approaches the fractal value 1.9, which is close to the fractal dimension of two-dimensional percolation.[34] As will be discussed below this limit is not uniquely defined.

Before we discuss how the results depend on the particle concentration, we shall briefly make a note about the mechanism that is responsible for the formation of fractal domains during the irreversible growth process of the present model at zero temperature. This mechanism may

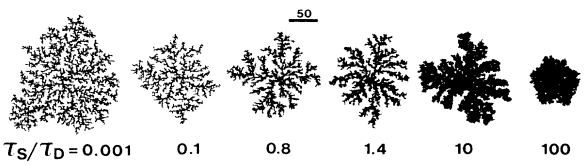

FIG. 2. Typical solid aggregates grown at zero temperature to a size of about 150 lattice units for particle concentration $\langle \eta_i \rangle = 0.3$ at time-scale ratios $\tau_S/\tau_D = 0.001$, 0.1, 0.8, 1.4, 10, and 100. The aggregates consist of about 10 000, 5500, 6200, 7000, 13 000, and 5000 particles, respectively. The solid bar indicates 50 lattice units.

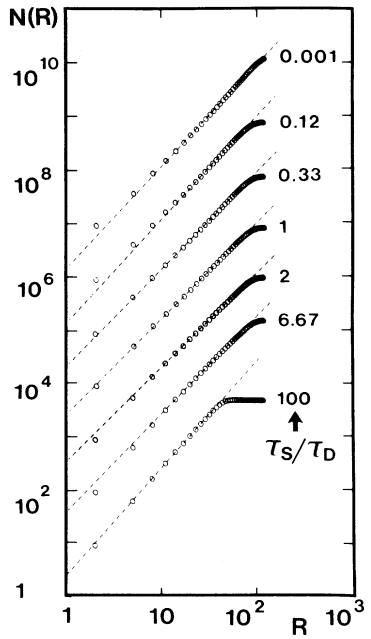

FIG. 3. Log-log plot of the particle content $N(R)$ vs linear dimension R of zero-temperature aggregates of the type displayed in Fig. 2. The particle concentration is $\langle \eta_i \rangle = 0.3$ and the time-scale ratio is given by τ_S/τ_D. For the sake of clarity, each data set has been shifted one decade upwards relative to the one below. The dotted lines symbolize fits to Eq. (6). The results are obtained by averaging over 10–15 aggregates.

be revealed[29] by studying the spatial distribution of vacancies as the growing domain evolves in time. It is then found that the vacancy distribution is not uniform but there is a distinct region depleted of particles in the active growth zone.[29] Consequently, it is the diffusional characteristics of the vacancies which determine the stability of

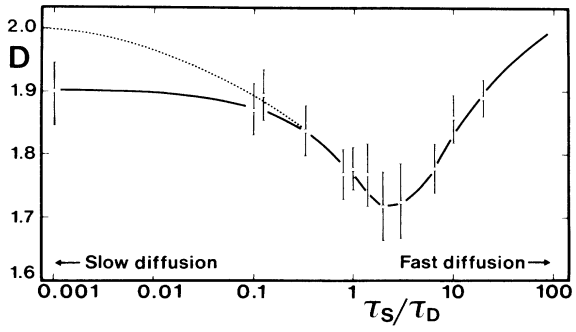

FIG. 4. Semilogarithmic plot of the zero-temperature fractal dimension D, Eq. (6), vs time-scale ratio τ_S/τ_D at particle concentration $\langle \eta_i \rangle = 0.3$. The plotted points are obtained by averaging over 10 to 15 samples. The heavy solid line is meant as a guide to the eye. The dotted line indicates for slow diffusion the crossover to the cluster-cluster aggregation regime.

the solidification front and hence the morphology of the aggregate. This depletion layer plays a role similar to that of the screening effect in DLA.[1]

The data reported so far refer to a particle concentration of $\langle \eta_i \rangle = 0.3$. We have obtained similar sets of data for particle concentrations in the range from $\langle \eta_i \rangle = 0.05$ to 0.50 with the following systematic trend: As $\langle \eta_i \rangle$ is decreased, the value of D decreases and approaches about 1.70. This is expected since in the limit of vanishing particle concentration, our model reduces to standard DLA. From the multiparticle DLA model studies by Meakin and Deutch[13] and Voss[14] it was argued that at finite particle concentrations the aggregates are fractal only up to a certain correlation length (which depends on the particle concentration) beyond which the aggregate attains the Euclidean dimension. These authors found a crossover from $D \simeq 1.7$ to $D = d = 2$ as the particle concentration is increased. The aggregates we have grown according to our model for particle concentrations up to $\langle \eta_i \rangle = 0.30$ show at moderate values of τ_S/τ_D no sign of a crossover to $D = 2$, not even for aggregates with a radius of up to 100 lattice units. Hence we have no indication of our aggregates not being fractal for moderate values of τ_S/τ_D. However, we cannot exclude that such a crossover may be present at larger length scales.

Turning now to the interesting limits of slow and fast diffusion, cf. Figs. 3 and 4, we first note that for fast diffusion there is a crossover to compact growth, $D \simeq 2$. In this limit the diffusion is so fast that it prevents a depletion layer being formed; the particle concentration is uniform right up to the solidification front. Hence the growth probability is uniform at the surface of the growing aggregate and the growth becomes stable. This is the limit of the Eden model.[35] The opposite limit of very slow diffusion is more complex. For zero diffusion the solid will grow in a stationary matrix of vacancies and since we are generally below the percolation limit, there is a finite probability that growth will stop at some time and the aggregate will be a finite percolation cluster. As soon as the diffusion is turned on, the aggregate can grow again. On the slow time scale of the diffusion, the growth will then occur in a stepwise fashion by solidifying and adding very rapidly whole percolation clusters whenever these, via a diffusive link, become connected to the current solid aggregate. These percolation clusters may, again on the time scale of the slow diffusion, be seen as latent superparticles which diffuse around in the background and the growth resembles that of cluster-cluster aggregation.[4] This will lead to a structure which at long-length scales has a uniform density, but at short-length scales has the scaling properties of percolation clusters. This is fully consistent with the data in Fig. 4 which, for small values of τ_S/τ_D, suggests that D is close to 1.9 but for $\tau_S/\tau_D = 0.001$ there is a weak tendency for a crossover to $D = d$ at long-length scales. Hence the limit of vanishing diffusion is not uniquely defined, as also indicated on Fig. 4.

V. MULTIFRACTALITY AT ZERO TEMPERATURE

Obviously a detailed description of the morphology of objects such as those displayed in Fig. 2 in terms of a single fractal dimension D is very incomplete. A much more detailed characterization can be provided using the concepts of multifractality.[36,37] In view of the strong current interest in understanding a possible universal classification scheme of multifractal spectra[38–45] we shall here analyze the zero-temperature fractal domains in terms of multifractals. The multifractal formalism operates on the basis of a distribution of fractal dimensions which in turn requires a probability measure to be associated with the fractal set. This probability measure is discretized by assigning probabilities P_i to each box of linear dimension l belonging to a box covering of the fractal object. From the probability measure we define a set of generalized fractal dimensions[46] D_q defined by

$$D_q = \frac{1}{q-1} \lim_{l \to 0} \frac{\ln \sum_i P_i^q}{\ln l} . \tag{7}$$

The multifractal spectrum is related to the generalized dimensions through the equations[36,37]

$$\alpha(q) = \frac{d}{dq}[(q-1)D_q] \tag{8}$$

and

$$f(\alpha) = q\alpha(q) - (q-1)D_q . \tag{9}$$

Here, α is an index governing the scaling properties of the probability P_i assigned to the box, $P_i \sim l^{\alpha}$. The fractal set S is then defined as the union of fractal sets, S_α, each characterized by a scaling index α and a fractal dimension $f(\alpha)$, where α assumes a range of values between $\alpha_{\min}$ and $\alpha_{\max}$. The $f(\alpha)$ curve is bell shaped with positive values for $\alpha_{\min} < \alpha < \alpha_{\max}$. The maximum of the curve corresponds to $f(\alpha(0)) = D_0$, the fractal dimension of the set, and the two values $\alpha_{\min}$ and $\alpha_{\max}$ correspond to D_∞ and $D_{-\infty}$, respectively. It can be shown[37] that the $f(\alpha)$ curve is tangential to the curve $f(\alpha) = \alpha$ at $\alpha(1) = D_1$.

In the case of the growing aggregates considered in this paper, the relevant probability measure is the surface growth-probability measure (SGPM). For this measure, the $f(\alpha)$ curve has a number of properties. Firstly, D_0 becomes the fractal dimension of the surface of the aggregate which in the case of a volume fractal should be equal to the fractal dimension of the whole set, S. Secondly, it has been shown that $\alpha(\infty) = D_\infty \leq D_0 - 1$.[47] Thirdly, as pointed out above, $f(\alpha)$ is tangential to the curve $f(\alpha) = \alpha$ at $\alpha(1) = D_1$. In the case of the harmonic measure (see below) it has been shown[48] that $D_1 = 1$. Thus the $f(\alpha)$ curve passes through the point (1,1).

Having established the necessary elements of the multifractal formalism, it remains to describe how one obtains the probabilities P_i from the SGPM. In the case of DLA there is a straightforward procedure.[41,43] The fractal surface is probed by a number N of independent random walkers and the number of times N_i each surface site is visited is recorded. The probabilities are then taken to be $P_i = N_i/N$. This is equivalent to the harmonic measure obtained by solving the Laplace equation numerically on a lattice. The advantage of the method using

random walkers to derive the harmonic measure is that it is straightforward to apply to large aggregates. It has the drawback of providing poor estimates of the spectrum for $q<0$ since very few walkers visit the deep interior of the fjords.[43]

In order to determine the multifractal spectrum for the present zero-temperature aggregates we have made use of a special version of the random-walker probing method by employing 50 000 probes simultaneously. It should be noted, however, that the relationship between the SGPM determined in this way and the harmonic measure is unclear since our algorithm does not provide a direct solution to the Laplace equation. Our algorithm is implemented in the following way. An aggregate is grown to a certain size. The growth is then stopped but the dynamics carries on. Instead of sticking the particles to the surface of the aggregate, counters at each surface site measure how many times particles are visiting that site. Every time such an event occurs, the particle is removed and reintroduced at random at the boundary of the lattice. Figure 5 illustrates how the fractal surface is probed by this method.

From the probability measure P_i obtained in this way D_q is readily obtained from Eq. (7) using a box counting algorithm. As already pointed out this will lead to unreliable estimates of the spectrum for $q<0$ as can be seen in Fig. 6. However, instead of neglecting points at the fractal surface which are not reached by any of the $N=50\,000$ probes, we assign an approximate probability $P_i=N^{-1}$ to these points, which is an upper limit to the correct value of P_i. The set of P_i is then adjusted to fulfill the normalization condition, $\sum_i P_i=1$. The data obtained from such a correction procedure are shown in Figs. 6–8 for different values of τ_S/τ_D. From these figures it is observed that D_0 now closely corresponds to

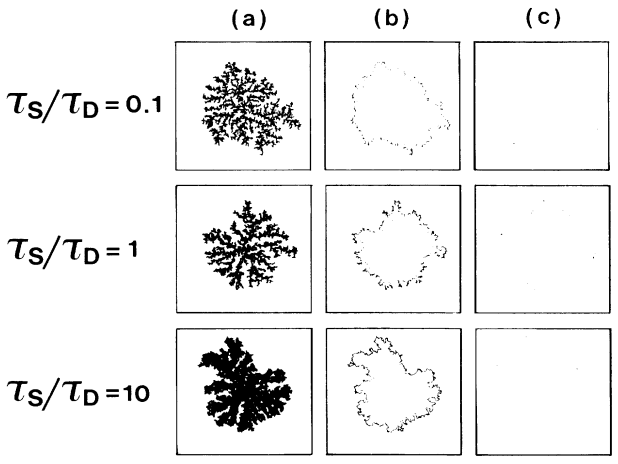

FIG. 5. Fractal aggregates (a) grown at zero temperature and their probability measures (b) and (c). (b) shows particles of the aggregates which have been hit at least once, and (c) shows particles which have been hit at least 100 times. The particle concentration is $\langle \eta_i \rangle = 0.3$.

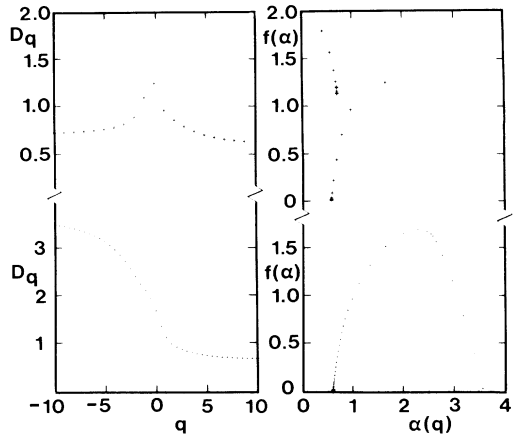

FIG. 6. Set of fractal dimensions D_q, Eq. (7), and corresponding fractal spectrum $f(\alpha)$, Eq. (9), where α is the scaling index, Eq. (8). The data refer to the zero-temperature aggregates in Fig. 5 at $\tau_S/\tau_D=0.1$. The particle concentration is $\langle \eta_i \rangle = 0.3$. The upper curves represent the raw data. In the lower curves, the data have been subject to the corrections described in the text in order to access the $q<0$ regime.

the fractal dimension of the set and the $f(\alpha)$ curve passes through (1,1) as expected for the harmonic measure. Also the relation $D_\infty < D_0 - 1$ is obeyed. However, it should be emphasized that the $q<0$ part of the D_q spectrum which corresponds to the right-hand side of the $f(\alpha)$ spectrum should merely be taken as a rough guideline, considering the approximations being used. Still, the values obtained are similar to those obtained from DLA-type growth models, e.g., the screened-growth cluster model,[43] where the harmonic measure can be estimated by other methods.

Comparing the corrected D_q spectra in Figs. 6–8 for different values of τ_S/τ_D it is observed that D_q on both sides of $q=0$ approaches the line $D_q=1$ as the diffusion gets faster. This is consistent with our findings in Sec. IV

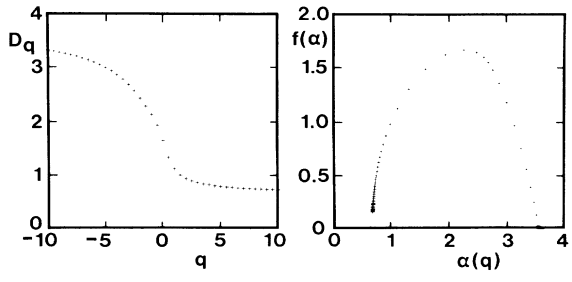

FIG. 7. Set of fractal dimensions D_q, Eq. (7), and corresponding fractal spectrum $f(\alpha)$, Eq. (9), where α is the scaling index, Eq. (8). The data, which refer to the zero-temperature aggregates in Fig. 5 for $\tau_S/\tau_D=1$, have been subject to the corrections described in the text. The particle concentration is $\langle \eta_i \rangle = 0.3$.

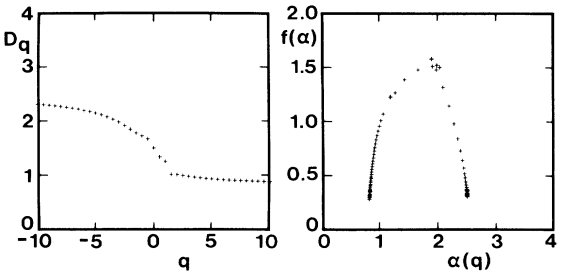

FIG. 8. Set of fractal dimensions D_q, Eq. (7), and corresponding fractal spectrum $f(\alpha)$, Eq. (9), where α is the scaling index, Eq. (8). The data, which refer to the zero-temperature aggregates in Fig. 5 for $\tau_S/\tau_D=10$, have been subject to corrections described in the text. The particle concentration is $\langle \eta_i \rangle = 0.3$.

which show that the model in the fast-diffusion limit approaches the Eden model which has $D_q=1$ and an $f(\alpha)$ curve reduced to the single point (1,1).

Our data on multifractal properties of the present model are too imprecise and cover a too limited range of τ_S/τ_D values to permit some very strong conclusions. However, we have established that it is possible to extend the multifractal formalism to work for growth models of the present type. Our results for the $f(\alpha)$ spectrum are very similar to those obtained for DLA-type models and we conclude that the present growth model belongs to the universality class of DLA.

VI. FINITE-TEMPERATURE RESTRUCTURING AND CROSSOVER FROM NONEQUILIBRIUM GROWTH TO EQUILIBRIUM COMPACTIFICATION

We now lift the zero-temperature condition which leads to the irreversible growth phenomena described in Secs. IV and V. By allowing for thermal activation we permit particles which once have aggregated and solidified to detach and fluidize again and therefore also diffuse again. This will lead to a temperature-dependent morphology at early times and will in the late-time regime eventually lead to restructuring, compactification, and crossover to an equilibrium structure or an equilibrium stable growth situation. Obviously, the present model is rather rich with a large parameter space. For practical reasons we have for the present restricted ourselves to study part of this space, and the results described in this section are obtained on a 256×256 lattice for a single time-scale ratio, $\tau_S/\tau_D=1$, and in most cases the particle concentration is $\langle \eta_i \rangle = 0.1$.

A. Crossover in temperature

Firstly, we describe the temperature-dependent growth phenomena in the early-time regime where diffusion of particles is an important regulator of the growth process. In Fig. 9 are shown typical configurations at time $t=5000$ MCS/S obtained for several different growth temperatures. The first nucleation event is always taken to define the center of the simulational box. Since the full features of the Hamiltonian model now come into play at finite temperatures, spontaneous nucleation occurs in several places, cf. Fig. 9, especially at low temperatures. At higher temperatures, often only a single nucleation center survives and grows persistently within the time regime studied. The depletion layers are clearly visible and so are the distortion effects caused by the interaction between depletion layers from different growing domains. The higher the temperature, the less pronounced is the depletion layer and at the same time the domains grow thicker fingers, restructure, and compactify. At the highest temperatures in Fig. 9 the depletion layer is absent and the growth has attained a stable situation within the studied time span. Hence Fig. 9 shows a distinct crossover from fractal growth to compact growth in the early-time regime. The shape of the solid domains at high temperatures is clearly influenced by the underlying square-lattice structure.

The crossover in temperature is quantified by calculating the fractal exponent, cf. Eq. (6), at different temperatures.[29] Since several aggregates and domains may be present at the same time, such a calculation is most conveniently carried out by computing the number of solidified particles $N(R_g)$ in each cluster versus its radius of gyration R_g and then deriving D from the relationship

$$\ln N(R_g) \sim D \ln R_g \tag{10}$$

for all clusters. Since larger values of R_g for a given cluster correspond to a longer time lapse since its nucleation, such a procedure will only work if an insignificant amount of restructuring takes place within the studied time span. In fact, it turns out that for $t \leq 5000$ MCS/S, only single-bonded particles are found to detach due to

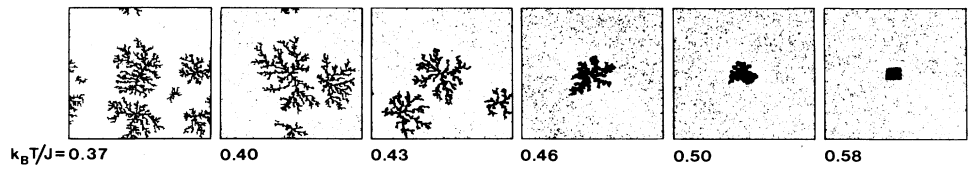

FIG. 9. Typical configurations in the early-time regime, $t=5000$ Monte Carlo steps per site (MCS/S), for different values of the growth temperature. The particle concentration is $\langle \eta_i \rangle = 0.1$. Both fluid and solid particles are denoted by black dots. The connected structures are solid domains. The lattice contains 256×256 sites.

thermal fluctuations. Hence no major restructuring takes place in the early-time regime. The thermal fluctuations therefore correspond effectively to lowering the sticking probability which leads, as observed, to a finger thickening of the fractal domains. By averaging over 10–70 runs, depending on the temperature, D is obtained as a function of temperature as shown in Fig. 10. This figure reveals a smooth crossover from a DLA-like fractal exponent value, $D \simeq 1.76 \pm 0.02$, at low temperatures to a value $D \simeq 2.00 \pm 0.01$ characteristic of compact domains for $k_B T/J \geq 0.58$.

An inset in Fig. 10 shows at a selected (low) temperature at $t = 5000$ MCS/S how the effective fractal dimension decreases towards the DLA value as the particle concentration is lowered.

Since our model is formulated on the basis of an energy function, an alternative and more physical characterization of the crossover from fractal to compact morphology may be provided in terms of the effective time-dependent coordination number

$$z(t) = |H(t)|/N(t) \tag{11}$$

defined as the ratio of the total domain energy to the number of solid particles in the domain. Due to the assumption $E_{-1} = 0$ only solid-solid pair-interaction contributions are included in the total domain energy. In Fig. 11, $z(t)$ is plotted for different temperatures. Note the crossover in temperature, at a given time, of $z(t)$ towards the value $z = 4$ of a compact domain on the square lattice. The substantial scattering in the data at very early times is due to the smallness of the domains shortly after their nucleation.

B. Temporal scaling in the early-time regime

At low temperatures in the early-time regime where the growth of the solid domains is mainly diffusion limited we can describe the time evolution of the fractal domains by a simple expression based on scaling arguments.[22] In the active growth zone, which is at a distance

$$R_g(t) \sim N^{1/D}(t) \tag{12}$$

from the center of the aggregate, the particle density scales as

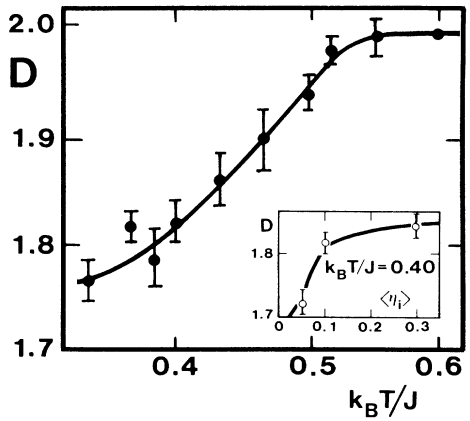

FIG. 10. Fractal dimension D as a function of growth temperature in the early-time regime, $t = 5000$ MCS/S, cf. Fig. 9, for particle concentration $\langle \eta_i \rangle = 0.1$. The inset shows for a selected temperature, $k_B T/J = 0.40$, how D varies with particle concentration $\langle \eta_i \rangle$.

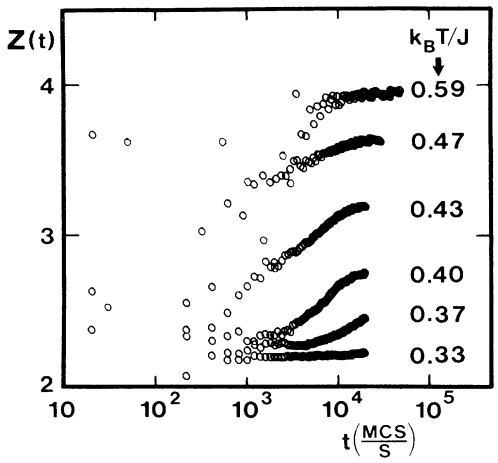

FIG. 11. Plot of effective coordination number $z(t)$ vs time t for different growth temperatures in the early-time regime. The effective coordination number is defined by Eq. (11).

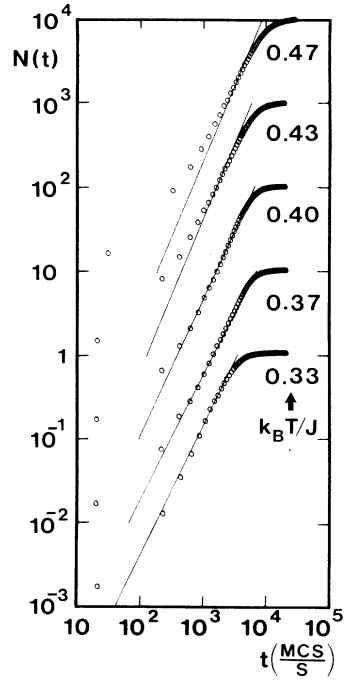

FIG. 12. Double-logarithmic plot of the particle content $N(t)$ of particles in solid domains vs time t at different growth temperatures in the low-temperature region. The early time regime, $t \leq 5000$ MCS/S, which is dominated by diffusion-limited growth at low temperatures, is described by the scaling law, Eq. (15), shown as the solid lines.

$$\rho(R_g) \sim R_g^{D-d} . \tag{13}$$

The change in particle content in the growth zone can be described by the differential equation

$$\frac{dN(t)}{dt} \sim [\rho(R_g(t))]^2 R_g(t) , \tag{14}$$

which using Eqs. (12) and (13) has the solution

$$N(t) \sim t^{D/(2d-D-1)} . \tag{15}$$

Equation (15) expresses a temporal scaling behavior in the diffusion-limited early-time regime. In Fig. 12 are shown the numerical-simulation data for $N(t)$ in the early-time regime for different growth temperatures together with the scaling prediction, Eq. (15). The values of D used for the theoretical plots are those given in Fig. 10. It is seen that for low temperatures, $k_B T/J \leq 0.40$, where there is only an insignificant restructuring and finger thickening, the data is well described by the temporal scaling relation. At higher temperatures the assumption of diffusion-limited growth breaks down and there is a crossover to high-temperature stable growth as described in Sec. VI C.

It should be noted that it is not possible to write an equation of the type of Eq. (14) in terms of local densities in the case of standard DLA.[49] For two-dimensional DLA there are no steady-state solutions to the diffusion equation[49] and one is expected to find $N(t) \sim t$, possibly with logarithmic corrections.

C. Stable growth at high temperatures

At high temperatures the thermal fluctuations overrule the diffusional motion at the solidification front. The aggregation probability is then effectively uniform at the surface and the growth becomes stable. For not too high temperatures where the detachment rate is slow, we can describe this regime approximately by the differential equation

$$\frac{dN(t)}{dt} = a c(t) s(t) , \tag{16}$$

where $c(t)$ is the concentration of fluid particles and $s(t)$ is the surface (perimeter) of the growing aggregate, $s(t) \sim \sqrt{N(t)}$. The concentration $c(t)$ can be written

$$c(t) = \frac{\langle \eta_i \rangle N_s - N(t)}{N_s - N(t)} \approx \frac{\langle \eta_i \rangle N_s - N(t)}{N_s} , \tag{17}$$

where N_s is the total number of lattice sites. The indicated approximation in the second part of Eq. (17) holds when the aggregated solid is small compared with the total system size. We shall use this approximation in the following, since the solid occupies no more than 10% of the total system. Equations (16) and (17) then imply

$$\frac{dN(t)}{dt} = a \frac{\langle \eta_i \rangle N_s - N(t)}{N_s} \sqrt{N(t)} , \tag{18}$$

which has as its solution

$$\tilde{N}(t) = \frac{N(t)}{\langle \eta_i \rangle N_s} = \tanh^2 \left[\frac{a}{2} \left[\frac{\langle \eta_i \rangle}{N_s} \right]^{1/2} t \right] . \tag{19}$$

Equation (19) is inverted to give

$$at = 2 \left[\frac{N_s}{\langle \eta_i \rangle} \right]^{1/2} \tanh^{-1} \left[\frac{N(t)}{\langle \eta_i \rangle N_s} \right]^{1/2} . \tag{20}$$

Obviously, Eq. (19) obeys $\lim_{t \to \infty} N(t) = \langle \eta_i \rangle N_s$.

The constant a of the expression above depends on temperature and it is determined from the data by inserting into Eq. (20) the numerical data for $N(t)$, cf. the inset of Fig. 13. It is seen that Eq. (20) provides a satisfactory description of the data at early times. At later times there is a progressive deviation due to the breakdown of the approximation, Eq. (17). Inserting the values found for a back into Eq. (19) we find the very satisfactory correlation in Fig. 13 between the numerical data for $N(t)$ and the theoretical prediction. As expected, this correlation becomes less good as the temperature is increased.

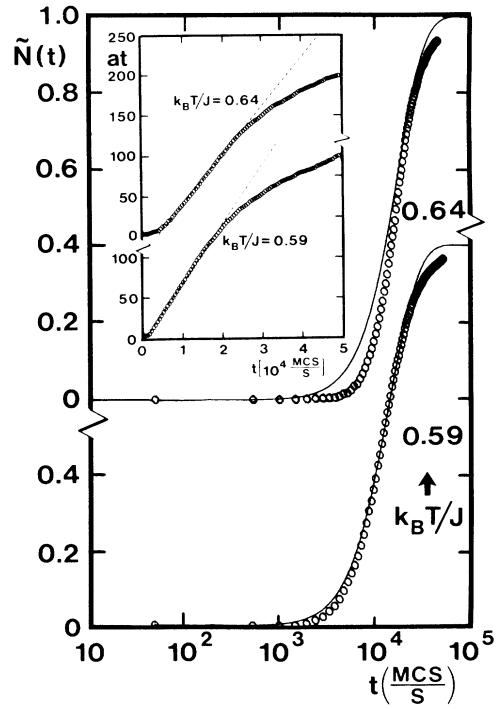

FIG. 13. Semilogarithmic plot of the normalized particle content $\tilde{N}(t)$ of particles in solid domains vs time t at two different growth temperatures in the high-temperature region. The high-temperature region is approximately described by the differential equation, Eq. (18), which leads to the hyperbolic tangent relation, Eq. (19), which is plotted as solid lines. The parameter a determining the width of the hyperbolic function is obtained from the fits in the inset which are obtained according to Eq. (20).

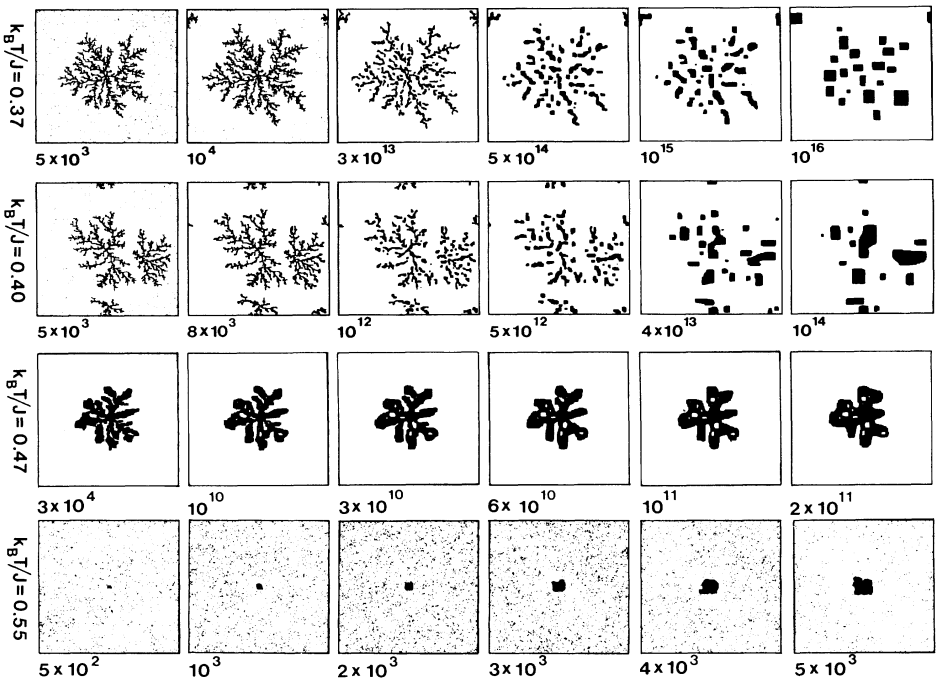

FIG. 14. Typical configurations at different times in the late-time regime shown for different growth temperatures. The particle concentration is $\langle \eta_i \rangle = 0.1$. The value of the time parameter t (in units of MCS/S) is displayed below each snapshot. Both fluid and solid particles are denoted by black dots. The connected structures are solid domains. The lattice contains 256×256 sites.

D. Crossover in time

In Fig. 14 typical configurations for different temperatures are shown as they evolve in time over up to about 12 decades. Such a time study is only feasible because of our use of the continuum-time method described in Sec. III. As time elapses at the lower temperatures, $k_BT/J=0.37$ and 0.40, all of the particles solidify, the tenuous structures break up, and restructuring occurs via melting. The resulting fragments eventually compactify. This final stage, which is akin to a sintering process, is extremely slow, $N(t)\sim t^{0.03}$ [or possibly $N(t)\sim \ln t$], and it leads to the formation of a single solid domain (not shown in Fig. 14). At a higher temperature, $k_BT/J=0.47$, the fractal collapses without appreciable fragmentation. At even higher temperatures, e.g., $k_BT/J=0.55$, the domains grow in a compact fashion from a very early stage.

The overall result from Fig. 14 is the finding of a crossover in time from early-time fractal growth to late-time compactification. The higher the temperature is, the earlier in time the crossover occurs. Since the type of tenuous patterns seen at low temperatures in Fig. 14 make it difficult to define a measure of the morphology and its possible scaling properties, it is not feasible to quantitatively analyze this late-time morphology as a function of time.

VII. DISCUSSION

We have in this paper described the results of the first study of the crossover from nonequilibrium fractal growth to equilibrium compact growth by using a Hamiltonian formalism which permits definition of a thermodynamic temperature. Most theoretical and numerical studies of fractal growth are usually carried out by means of models which embody an intrinsic irreversibility and hence do not provide equilibrium conditions in any thermodynamic sense. The model used in the present work is a special version of the two-dimensional site-diluted spin-$\frac{1}{2}$ Ising model which describes a thermally driven solidification on a lattice in terms of internal single-site degrees of freedom. It is the diffusional characteristics of the mobile vacancies at the solidification front which at low temperatures and early times lead to formation of solid domains with an effective fractal morphology. As the temperature is raised or the time region studied is expanded, we observe a distinct crossover to compact growth.

The results presented in this work were obtained at high dilution. It is possible that the zero-temperature tenuous structures found here are only fractal at finite length scales and that true fractals of infinite correlation are only obtained for infinitely high dilution (the DLA limit). Still we wish to emphasize that for all practical purposes many of the tenuous structures found in our model study are effectively fractals and that the interesting observation is that such structures decay into compact domains as equilibrium is approached.

The present model study was stimulated by the experimental observations in lipid monolayers of nonequilibrium fractal solidification.[27,28] In these experiments, which are carried out on a monomolecular film on an air-water

interface doped with a fluorescent dye impurity only miscible in the fluid phase, the solidification is induced by a rapid lateral compression. In agreement with the experimental observation of an enhanced level of dye impurities in the active growth zone, we find in our model, where the vacancies take on the role of the impurities, that there is a depletion of fluid material at the solidification front. That it is the fluctuations in this depletion layer which are the main mechanism responsible for formation of fractal domains is underlined by the fact that in the experimental system there is a strong and fast thermocoupling between the lipid monolayer and the water subphase. Hence diffusion of latent heat cannot be held responsible for the surface instabilities.

ACKNOWLEDGMENTS

This work was supported by the Danish Natural Science Research Council under Grant Nos. 5.21.99.72 and 11-6836. Enlightening discussions with Bill Klein and Heinrich Röder are gratefully acknowledged.

[1]T. A. Witten and L. M. Sander, Phys. Rev. B **27**, 5686 (1983).
[2]I. Procaccia and R. Zeitak, Phys. Rev. Lett. **60**, 2511 (1988).
[3]T. Bohr, P. Cvitanović, and M. H. Jensen, Europhys. Lett. **6**, 445 (1988).
[4]See, e.g., papers in the book *On Growth and Form. Fractal and Non-Fractal Patterns in Physics*, edited by H. E. Stanley and N. Ostrowsky (Nijhoff, Boston, 1986).
[5]T. Freltoft, J. K. Kjems, and S. K. Sinha, Phys. Rev. B **33**, 269 (1986).
[6]C. Aubert and D. S. Cannell, Phys. Rev. Lett. **56**, 738 (1986).
[7]P. Dimon, S. K. Sinha, D. A. Weitz, C. R. Safinya, G. S. Smith, W. A. Varady, and H. M. Lindsay, Phys. Rev. Lett. **57**, 595 (1986).
[8]O.-Y. Zhong-can, Y. Gang, and H. Bai-lin, Phys. Rev. Lett. **57**, 3203 (1986).
[9]J. Nittmann and H. E. Stanley, Nature (London) **321**, 663 (1986).
[10]E. Ben-Jacob, G. Deutscher, P. Garik, N. D. Goldenfeld, and Y. Lareah, Phys. Rev. Lett. **57**, 1903 (1986).
[11]F. Family, D. E. Platt, and T. Vicsek, J. Phys. A **20**, L1177 (1987).
[12]J. Nitttmann and H. E. Stanley, J. Phys. A **20**, L1185 (1987).
[13]P. Meakin and J. M. Deutch, J. Chem. Phys. **80**, 2115 (1984).
[14]R. F. Voss, Phys. Rev. B **30**, 334 (1984).
[15]Y.-B. Huang and P. Somasundaran, Phys. Rev. A **36**, 4518 (1987).
[16]R. Jullien, M. Kolb, and R. Botet, J. Phys. (Paris) **45**, 395 (1984).
[17]J. Kertész and T. Vicsek, J. Phys. A **19**, L257 (1986).
[18]J. R. Banavar, M. Kohmoto, and J. Roberts, Phys. Rev. A **33**, 2065 (1986).
[19]K. K. Mon, Phys. Rev. A **34**, 4469 (1986).
[20]R. Tao, M. A. Novotny, and K. Kaski, Phys. Rev. A **38**, 1019 (1988).
[21]P. M. Mors, R. Botet, and R. Jullien, J. Phys. A **20**, L975 (1987).
[22]E. S. Sørensen, H. C. Fogedby, and O. G. Mouritsen, Phys. Rev. Lett. **61**, 2770 (1988).
[23]W. Y. Shih, I. A. Aksay, and R. Kikuchi, Phys. Rev. A **36**, 5015 (1987).
[24]R. Botet and R. Jullien, Phys. Rev. Lett. **55**, 1943 (1985).
[25]M. Kolb, J. Phys. A **19**, L263 (1986).
[26]L. Monette, W. Klein, M. J. Zuckermann, A. Khadir, and R. Harris, Phys. Rev. B (to be published).
[27]A. Miller, W. Knoll, and H. Möhwald, Phys. Rev. Lett. **56**, 2633 (1986).
[28]A. Miller and H. Möhwald, J. Chem. Phys. **86**, 4258 (1987).
[29]H. C. Fogedby, E. S. Sørensen, and O. G. Mouritsen, J. Chem. Phys. **87**, 6706 (1987).
[30]O. G. Mouritsen, H. C. Fogedby, E. S. Sørensen, and M. J. Zuckermann, in *Time-Dependent Effects in Disordered Materials*, edited by R. Pynn and T. Riste (Plenum, New York, 1987), p. 457.
[31]S. Doniach, J. Chem. Phys. **68**, 4912 (1978).
[32]O. G. Mouritsen, *Computer Studies of Phase Transitions and Critical Phenomena* (Springer-Verlag, New York, 1984).
[33]A. B. Bortz, M. H. Kalos, and J. L. Lebowitz, J. Comput. Phys. **17**, 10 (1975).
[34]D. Stauffer, Phys. Rep. **54**, 1 (1979).
[35]Z. Rácz and M. Plischke, Phys. Rev. A **31**, 985 (1985).
[36]T. C. Halsey, P. Meakin, and I. Procaccia, Phys. Rev. Lett. **56**, 854 (1986).
[37]T. C. Halsey, M. H. Jensen, L. P. Kadanoff, I. Procaccia, and B. I. Shraiman, Phys. Rev. A **33**, 1141 (1986).
[38]M. H. Jensen, L. P. Kadanoff, A. Libchaber, I. Procaccia, and J. Stavans, Phys. Rev. Lett. **55**, 2798 (1985).
[39]P. Meakin, H. E. Stanley, A. Coniglio, and T. A. Witten, Phys. Rev. A **32**, 2364 (1985).
[40]C. Amitrano, A. Coniglio, and F. di Liberto, Phys. Rev. Lett. **57**, 1016 (1986).
[41]P. Meakin, A. Coniglio, H. E. Stanley, and T. A. Witten, Phys. Rev. A **34**, 3325 (1986).
[42]J. Nittmann, H. E. Stanley, E. Touboul, and G. Daccord, Phys. Rev. Lett. **58**, 619 (1987).
[43]P. Meakin, Phys. Rev. A **35**, 2234 (1987).
[44]S. Ohta and H. Honjo, Phys. Rev. Lett. **60**, 611 (1988).
[45]M. Blunt and P. King, Phys. Rev. A **37**, 3935 (1988).
[46]H. G. E. Hentschel and I. Procaccia, Physica D **8**, 435 (1983).
[47]F. Leyvraz, J. Phys. A **18**, L941 (1985).
[48]N. G. Makarov, Proc. London Math. Soc. **51**, 369 (1985).
[49]P. Meakin, in *Time-Dependent Effects in Disordered Materials*, edited by R. Pynn and T. Riste (Plenum, New York, 1987), p. 45.